IOP Publishing Superconductor Science and Technology
Supercond. Sci. Technol. 31 (2018) 095005 (10pp) https://doi.org/10.1088/1361-6668/aad275

Static and radio frequency magnetic response of high T_c superconducting quantum interference filters made by ion irradiation

Eliana Recoba Pawlowski[1], Julien Kermorvant[2], Denis Crété[1], Yves Lemaître[1], Bruno Marcilhac[1], Christian Ulysse[3], François Couëdo[4], Cheryl Feuillet-Palma[4], Nicolas Bergeal[4] and Jérome Lesueur[4]

[1] Unité Mixte de Physique CNRS, Thales, Université Paris-Sud, Université Paris-Saclay, 91 767 Palaiseau, France
[2] Thales Communication and Security, Gennevilliers, France
[3] Centre de Nanosciences et de Nanotechnologie, CNRS, Université Paris Saclay, Marcoussis, France
[4] Laboratoire de Physique et d'Etude des Matériaux, CNRS, ESPCI Paris, PSL Research University, UPMC, Paris, France

E-mail: jerome.lesueur@espci.fr

Received 26 February 2018, revised 26 June 2018
Accepted for publication 10 July 2018
Published 1 August 2018

Abstract

Superconducting quantum interference filters (SQIF) are promising devices for radio frequency (RF) detection combining low noise, high sensitivity, large dynamic range and wide-band capabilities. Impressive progress has been made recently in the field, with SQIF based antennas and amplifiers showing interesting properties in the GHz range using the well-established Nb/AlO_x technology. The possibility to extend these results to high temperature superconductors (HTS) is still open, and different techniques to fabricate HTS SQIFs compete to make RF devices. We report on the DC and RF response of a high temperature SQIF fabricated by the ion irradiation technique. It is made up of 1000 superconducting quantum interference devices in series, with loop areas randomly distributed between 6 and 60 μm^2. The DC transfer factor is $\sim 450\,V\,T^{-1}$ at optimal bias and temperature, and the maximum voltage swing ~ 2.5 mV. We show that such a SQIF detects RF signals up to 150 MHz. It presents linear characteristics for RF power spanning more than five decades, and non-linearities develop beyond $P_{RF} = -35$ dBm in our set-up configuration. The second harmonic generation has been shown to be at a minimum at the functioning point in the whole range of frequencies. A model has been developed which captures the essential features of the SQIF RF response.

Keywords: SQIF, SQUID, superconducting RF device, high Tc superconductors

(Some figures may appear in colour only in the online journal)

1. Introduction

To develop the next generation of analogue radio frequency (RF) front end devices in wireless communications and radar, an ultra wide bandwidth, compactness, high linearity, high sensitivity, and a large dynamic range are essential parameters. These characteristics are particularly difficult to simultaneously satisfy in conventional antennas. Indeed, such devices use a resonance to amplify the voltage induced at the antenna terminals by the incident electromagnetic wave. The resonance is usually obtained either by a specific geometrical configuration and/or by the development of a complex tuning network leading in both cases to a strong reduction of the operation bandwidth. One way to overcome the limitations of

classical antennas is the use of frequency independent sensitive devices such as superconducting quantum interference devices (SQUIDs), a superconducting loop interrupted by two Josephson junctions (JJ) [1]. They are highly sensitive to an applied magnetic flux over a very large bandwidth, from DC to tens of GHz depending on the technology used for the fabrication of the JJ. Moreover, since the magnetic field of the wave is detected, rather than the electric one as in a conventional RF detector, SQUIDs can have sub-wavelength sizes, and therefore be very compact, maintaining high sensitivity.

However, the use of a single SQUID to perform efficient RF detection is limited by the low voltage swing across the interferometer, leading to a reduced range of linearity and rather low transfer factor $\partial V/\partial B$ (V is the voltage and B the applied magnetic field). The latter can be enhanced either by a larger SQUID loop area or by the adjunction of a surrounding flux transformer or flux concentrator, at the expense of the dynamic range. Moreover, because of the periodic response of the SQUID to the magnetic flux, a feedback loop is mandatory to operate the device around a fixed functioning point and avoid flux jumps, which severely limit the bandwidth of the system as well [1].

In order to overcome those limitations, series arrays of N SQUIDs have been proposed as RF amplifiers [2–6]. Both the transfer factor and the voltage swing increase as a function of N while the output voltage noise increases as $\sqrt{N}$ and the flux noise decreases as $1/\sqrt{N}$, which is favourable. In arrays of identical SQUIDs the periodicity of the magnetic voltage response remains present. Arrays known as superconducting quantum interference filters (SQIFs) were proposed in this context, to perform an absolute measure of the magnetic field [7].

Since the pioneering work of Oppenlander *et al* [8, 9], SQIFs have appeared as promising devices for cryogenic electronics. A SQIF is an array of SQUIDs with loops of different sizes such that its response to an applied magnetic field is non-Φ_0 periodic, where $\Phi_0 = h/2e$ is the flux quantum. SQIFs belong to the growing family of superconducting devices based on multiple JJ arrays (see Cybart *et al* [10] and references therein for a review). The interest of SQIFs as compared to regular SQUID arrays lies in the single valued response to external magnetic field. This makes the realisation of highly sensitive absolute value magneto-sensors possible [11–14], and opens the door to high frequency compact detectors and low noise amplifiers (LNAs). The bandwidth of a SQIF is not limited by the feedback loop, but in principle by the gap of the superconductors which is an upper bound (up to a few THz for some materials), and by the electrodynamics of the JJ and the superconducting circuit (more in the hundreds of GHz range). As a consequence, SQIFs are very good candidates to detect and amplify RF waves.

In recent years, very promising results have been reported in the literature for high frequency devices based on SQIFs. Using Nb based technology, Kornev *et al* made pulse amplifiers or drivers in the context of rapid single flux quantum logic working at 100 MHz [15], and proposed advanced SQIF architectures for microwave applications in general [16]. Wide-band microwave LNAs with a power gain of 20 dB from 8 to 11 GHz [17], antennas in the near field [18] at 9 GHz and active electrically antennas [19] are being developed.

These devices work at the temperature of liquid helium. This limits their applications, and high Tc superconductors (HTS) appear to be good candidates to make RF devices with SQIFs. On one hand, with the operating temperature being higher, the cryogenics are simpler and cheaper. On the other hand, their superconducting gap is an order of magnitude larger than that of low Tc superconducting materials, and so this is the cut-off frequency of devices. Schultze *et al* successfully made the first HTS SQIF [12] that can be operated using commercial miniature cryocoolers [20]. In a first series of experiments, the JJs used in HTS SQIFs were fabricated using the so-called grain boundary junctions (GBJ) technology. Kornev *et al* [15] and Kalabukhov *et al* [21] reported a SQIF amplifier working at 100 MHz, while Shadrin *et al* [22] estimated a 20 dB power gain at 1–2 GHz. Caputo *et al* showed quadratic mixing using SQIFs up to 20 GHz [23, 24]. For practical reasons, it is difficult to make SQIFs with more than a few hundred loops with GBJ technology. Step-edge technology to fabricate HTS JJ is a very scalable process. Mitchell *et al* succeeded in producing high I_cR_n product JJ (I_c is the critical current and R_n is the resistance) with this technology [25]. The I_cR_n product sets the maximum operating frequency of the device through the Josephson relation $f_J = I_cR_n/\Phi_0$. Mitchell *et al* also recently operated a 20 000 JJ SQIF with a transfer factor $\partial V_{DC}/\partial B \sim 1500\ \mathrm{V\,T^{-1}}$ up to 30 MHz [26].

An alternative technology to make HTS SQUID arrays with a large number of JJ is irradiation technology [27, 28], developed both for DC and high frequency operations [29–31]. Large arrays have been produced [4, 32–34] with up to 36 000 JJ. We recently showed that a 4000 JJ SQIF can have a transfer factor $\partial V_{DC}/\partial B \sim 1000\ \mathrm{V\,T^{-1}}$ [35, 36] which is very encouraging. We present here the behaviour of such arrays at frequencies up to 200 MHz.

2. Experimental results

We designed and fabricated HTS SQIFs for DC and RF measurements using the ion irradiation technique. Details of the fabrication are described in previous papers [28, 35–38] and summarised here. We start with a commercial 150 nm thick c-axis oriented $YBa_2Cu_3O_7$ (YBCO) film (Ceraco GmbH) on a sapphire substrate covered by an *in situ* 100 nm thick gold layer to insure ohmic contacts. After removing the gold layer by Ar ion beam etching except on the contact pads, a photoresist is deposited on top of the YBCO layer to protect it from the subsequent ion irradiation, and patterned to define the superconducting parts of the SQIF and the RF loop (see figure 1(a)). A 110 keV oxygen ion irradiation at a dose of 5×10^{15} ions $\mathrm{cm^{-2}}$ is then performed which makes the unprotected part insulating. A polymethylmethacrylate resist is then deposited all over the sample, and narrow (40 nm

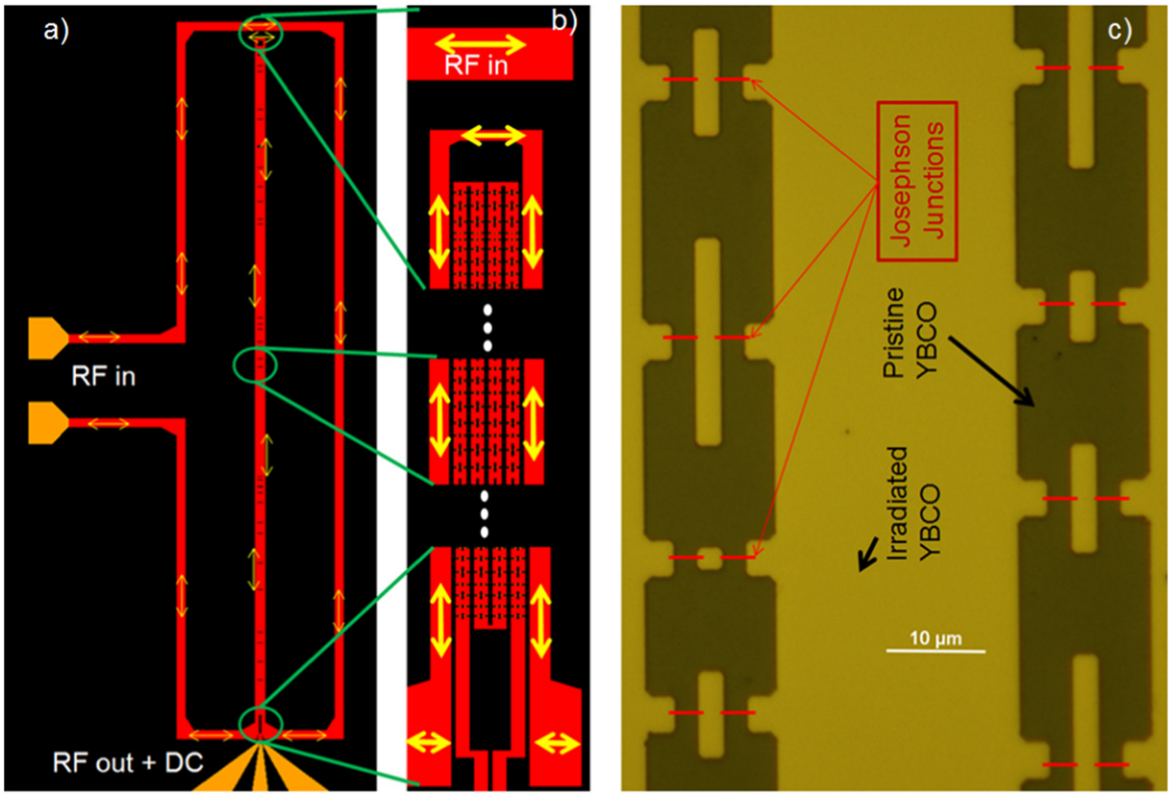

Figure 1. (a) Sketch of the device. A 1000 SQUID series SQIF is inserted within a RF loop. A RF signal is applied via the loop (gold contacts on the left), and detected by the SQIF (gold contacts at the bottom connected to a coplanar wave guides (CPW) line). (b) Enlargement of the central part of the device. The SQIF is folded into a meander line, and the input loop is placed along it. Yellow arrows symbolise the RF excitation current. (c) Optical picture of the central part of the SQIF which shows eight individual SQUIDs. Irradiated YBCO zones (light colour) are insulating after the first high dose irradiation. In a second step, JJ will be formed by low dose irradiation at the places shown by red lines.

wide) slits are opened across each arm of the superconducting loops (individual SQUIDs) by electron beam lithography. A second 110 keV oxygen ion irradiation performed at lower dose (3×10^{13} ions cm^{-2}) defines the JJ (see figure 1(c)). This fabrication technique is very flexible, scalable, and allows the realisation of large and complex structures. The one which is presented here is a 1000 SQUID series array SQIF, with loop areas ranging from 6–60 μm^2 with a pseudo-random distribution, folded in a meander line, which is surrounded by a RF line (figure 1) to induce AC current in the system. The width of the SQUID arms is 2 μm in the vicinity of the JJs. The total impedance of the SQIF is $\sim$200 Ω, larger than one needs to perfectly match the 50 Ω high frequency set-up measurement. This impedance matching problem limits the number of SQUIDs in series arrays to typically 1000 units. To go beyond this limit and enhance the SQIF behaviour, one has to arrange the SQUIDs in series and parallel.

To insure simultaneous DC and AC measurements, the sample is mounted on a printed-circuit board (PCB) with CPW lines for input and output RF signals, and DC pads. Short wire bonding between the sample and the PCB is then made, and the whole system is placed in a cryogen-free cryostat with no specific magnetic shielding. The external magnetic field is produced by Helmoltz coils mounted close to the sample. The RF signal is isolated from the DC part by a surface mounted bias-tee, pre-amplified at a low temperature (100 K), and measured with a spectrum analyser. The load impedance for the SQIF varies from 60–300 Ω in the frequency range that we used.

We first focused on DC characteristics of the SQIF. As reported earlier [36], the Josephson regime in such a device is observed below a coupling temperature $T_J \sim 73$ K, and extends over roughly 10 K. In this temperature range, the current–voltage (I–V) characteristics (figure 2) are typical of overdamped JJ with a slight deviation from the pure resistively shunted junction model, as known for ion irradiated YBCO JJ [29, 36, 38, 39]. The critical current I_c increases quadratically when lowering the temperature [28], while the normal state resistance R_n decreases. As a consequence, the I_cR_n product has a dome shape [29, 36], with a maximum value of $\sim$15 μV per SQUID. We applied a perpendicular magnetic field B on the device in the Josephson regime. A SQIF behaviour is observed under current bias larger than the critical current I_c: the voltage V_{DC} across the device presents a pronounced minimum around zero magnetic field (figure 3). Due to the unshielded environment, the minimum value $V_{\min}$ is not $B = 0$ exactly. The inset of figure 3 shows the voltage swing $\Delta V_{DC} = V_{DC} - V_{\min}$ as a function of B where the field offset has been subtracted. Hereinafter, this magnetic field offset has been systematically removed. The performance of the SQIF can be evaluated by the voltage swing

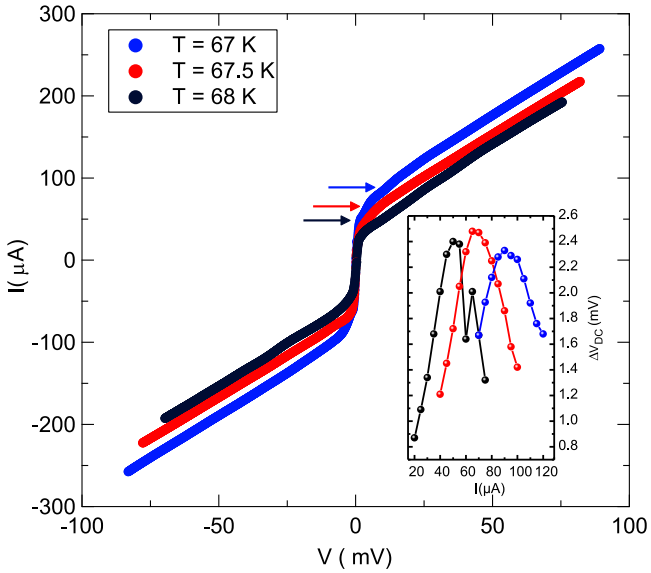

Figure 2. *I–V* characteristics of the 1000 SQUID series SQIF at different temperatures around the optimal temperature $T = 67.5$ K. Arrows indicate the optimal current I_{opt} for each temperature as defined in the inset. Inset: ΔV_{DC} of the device as a function of the bias current I for different temperatures. For each temperature there is an optimal bias I_{opt} for which ΔV_{DC} is maximum. I_{opt} also displays a maximum as a function of temperature. This figure shows that the optimal bias conditions are $T = 67.5$ K and $I = 65\ \mu A$.

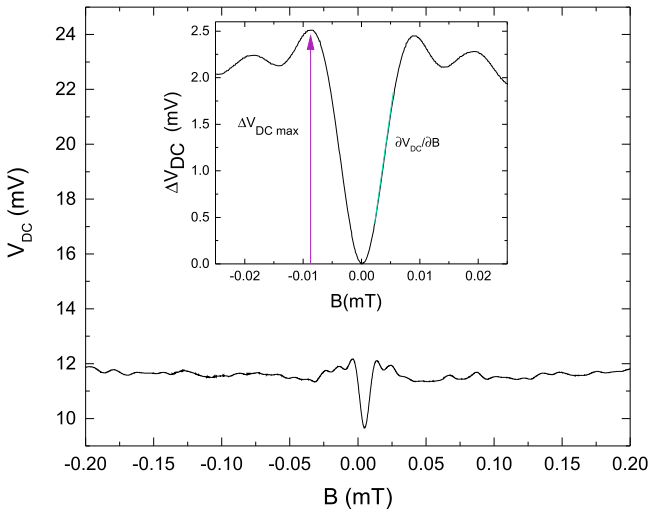

Figure 3. DC characterisation of the 1000 SQUID series SQIF. The output DC voltage V_{DC} as a function of the applied magnetic field B, for optimal bias ($I = 65\ \mu A$) and at optimal temperature ($T = 67.5$ K). The SQIF characteristic dip around $B = 0$ is observed. The minimum value $V_{\min}$ is not at $B = 0$ because of the offset field due to the unshielded environment. Inset: black curve: normalised plot of the data at low magnetic field: $\Delta V_{DC} = V_{DC} - V_{\min}$ as a function of B, where B is now the true field on the device after subtraction of the offset field. The maximum slope $V_B = |\partial V/\partial B|_{\max} \sim 450\ VT^{-1}$ (green line) and the maximum voltage swing $\Delta V_{DC\,\max} \sim 2.5$ mV (purple arrow).

$\Delta V_{DC\,\max} = \max(\Delta V_{DC})$ and the maximum transfer factor $V_B = |\partial V/\partial B|_{\max}$ at the inflexion point. In the inset of figure 2, we show the voltage swing ΔV_{DC} as a function of the applied bias current I for different temperatures. It has a pronounced maximum, which has itself a non-monotonic evolution with temperature. Therefore, there is a couple (current, temperature) for which ΔV_{DC} is maximum, as well as the transfer factor V_B, as shown in our previous work [35, 36]. The inset of figure 3 shows the ΔV_{DC} versus B curve corresponding to these optimal values ($T = 67.5$ K and $I = 65\ \mu A$): $\Delta V_{DC\,\max} \sim 2.5$ mV and $V_B \sim 450\ \mathrm{V\,T^{-1}}$ are roughly half the expected values already reported for a 2000 SQUID SQIF made in the same conditions [35, 36], and compare favourably with previous reports for HTS devices [20, 26].

It is worth mentioning that these values depend on the I_cR_n product of the individual SQUIDs in the SQIF. It is not possible to have such information for this device with thousands of junctions, but we know from previous studies the typical values for the I_cR_n products for ion irradiated JJ. The I_cR_n product is temperature dependent and its spread typically ranges from 7.5%–30% [40]. We recently studied an 18 SQUID SQIF where we could measure the individual SQUIDs, and model the SQIF behaviour from the measured characteristics. We confirmed the 30% spread in the I_cR_n products, and showed that this explains the SQIF DC response that we observed, and the values of V_B and $\Delta V_{DC\max}$ [36] as well.

When it comes to the maximum $\Delta V_{DC\max}$ possible, the comparison between SQIFs and arrays of identical SQUIDs is interesting. Recent simulations and experiments by Wu *et al* on HTS devices show that $\Delta V_{DC\max}$ is higher for an array of identical SQUIDs than for the equivalent SQIF [41]. This comes fundamentally from the fact that SQUIDs of different loop sizes have different inductances, and therefore different screening conditions. For a given set of operating conditions (bias current and temperature), not all of the SQUIDs of the array fully participate in the modulation of ΔV with the applied magnetic flux [36]. High values of $\Delta V_{DC\max}$ have been obtained with HTS regular SQUID arrays, up to 10.1 mV for a 770 SQUID array at 77 K for instance [6], which will be therefore difficult to achieve with SQIFs. However, the latter are still interesting for high frequency applications, thanks to their single valued response in magnetic flux.

We then measured the RF response of the sensor by superimposing a RF magnetic field and a slowly swept DC magnetic field B. A continuous wave input RF signal of frequency f_0 at a power level P_{RF} is applied through the superconducting planar loop. The DC (V_{DC}) and the amplified RF (V_{RF}) voltages are recorded simultaneously. In this study, the frequency f_0 ranges from 100 kHz to 200 MHz, and the input RF power P_{RF} from -85 dBm to -10 dBm.

Figure 4 shows V_{RF} (blue curve) and ΔV_{DC} (black curve) as a function of B in the optimal conditions (temperature and bias current) for $f_0 = 30.02$ MHz and $P_{RF} = -50$ dBm. The total magnetic field applied on the SQIF is $B_{tot} = B + b_{RF}\sin(2\pi f_0 t)$, where b_{RF} is the RF magnetic field amplitude proportional to the square root of P_{RF}. For a small b_{RF}, one can make a first order Taylor expansion of the output signal, and $V_{RF} \propto \partial\Delta V_{DC}/\partial B$. As expected in a linear regime, the RF signal appears as the derivative of the DC one, $\partial\Delta V_{DC}/\partial B$, which has been numerically calculated and

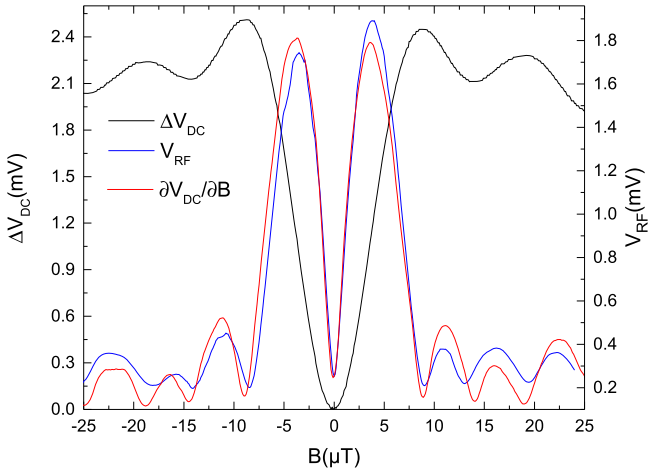

Figure 4. Simultaneous measurement of the DC ΔV_{DC} (black curve) and the amplified RF V_{RF} (blue curve) signals of a 1000 JJ series SQIF as a function of the magnetic field B. RF frequency is $f_0 = 30.02$ MHz and RF power is $P_{RF} = -50$ dBm. Temperature (67.5 K) and bias current (65 μA) correspond to optimal conditions. The red line shows the derivative $\partial\Delta V_{DC}/\partial B$, which matches the RF response as expected.

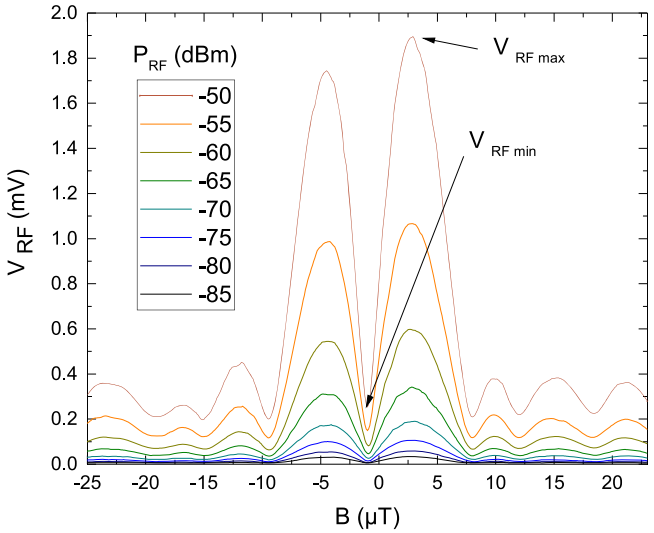

Figure 5. RF signal V_{RF} (amplified) of a 1000 SQUID series SQIF as a function of the magnetic field B for different RF powers from -85 dBm to -50 dBm. Temperature (67.5 K) and bias current (65 μA) are optimal. RF frequency is $f_0 = 30.02$ MHz. The maximum $V_{RF\max}$ and minimum $V_{RF\min}$ values are indicated by arrows.

shown in figure 4 (red curve). A detailed analysis and modelling of the data made in the last part of this article will point out non-linearities and the occurrence of an extra contribution to V_{RF} that cannot be simply extracted from the DC curve. The RF output signal increases with P_{RF} while keeping the same pattern as a function of the DC magnetic field B, in a wide range of input power, as shown in figure 5 for P_{RF} in the range -85 dBm to -50 dBm. To characterise the linearity of the SQIF response, we focused on the output power $P_{RFout} \propto V_{RF}^2$ at the optimum operating point. Interestingly, as seen in figure 4, this point corresponds both to the maximum of V_{RF} (called hereinafter $V_{RF\max}$) and the centre of the most linear part of the ΔV_{DC} versus B curve. Figure 6 shows

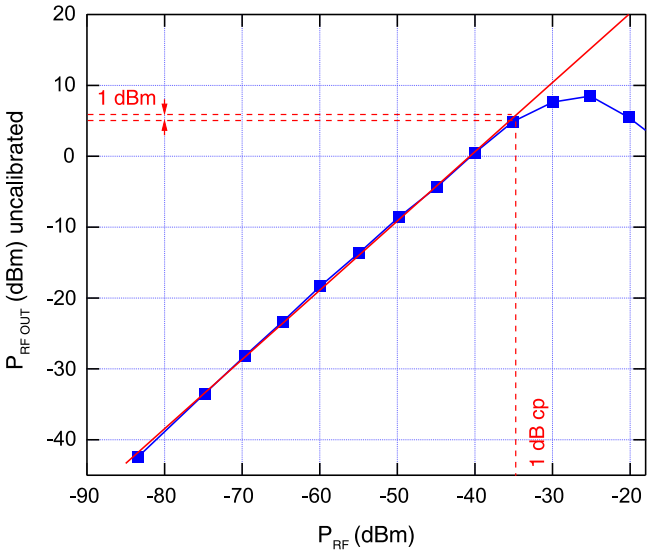

Figure 6. $P_{RF\text{out}}$ as a function of P_{RF} for a 1000 SQUID series SQIF. Temperature (67.5 K) and bias current (65 μA) are optimal. $P_{RF\text{out}}$ is the square of the maximum RF voltage $V_{RF\max}$, but uncalibrated. RF frequency is $f_0 = 10$ MHz and the RF power ranges from -85 dBm to -20 dBm. A linear behaviour is observed over five decades in RF power (red line). The one dB compression point is shown, setting the limit of the linear regime to -35 dBm.

$P_{RF\text{out}} \propto V_{RF\max}^2$ (expressed in dBm, not calibrated) as a function of P_{RF} for a frequency $f_0 = 10$ MHz. The linear behaviour extends on more than five decades, up to $P_{RF} = -35$ dBm (one dB compression point criteria). This result is valid for the whole range of frequencies studied here.

We increased the frequency up to $f_0 = 200$ MHz. For a constant RF input power $P_{RF} = -55$ dBm, the amplitude of the maximum output signal V_{RFmax} decreases as f_0 is increased, and dies out between 100 and 200 MHz, as seen in figure 7. This limitation may not be intrinsic to the HTS SQIF, since the RF circuitry is not fully optimised in this series of experiments. This result clearly shows that HTS SQIFs made by ion irradiation can operate at at least up to 150 MHz. The maximum operation frequency reported for a HTS SQIF made with step-edge JJ [26] is 30 MHz, while a GBJ based HTS SQIF can operate up to 100 MHz [15, 21].

Since the ΔV_{DC} versus B curve is essentially non-linear, it generates harmonics when the SQIF is submitted to an AC radiation. This is indeed observed as shown in figure 8. It is important to evaluate its contribution to the output signal. An input signal at $f_0 = 30.02$ MHz is sent and detected at twice the frequency $2 \times f_0 = 60.04$ MHz (blue line), and compared with $\partial^2\Delta V_{DC}/\partial B^2$ (red line). The agreement between the two is good, as expected. This behaviour is observed in the whole frequency range studied here. The frequency doubling is observed on a wide range of input powers typically below $P_{RF} \sim -35$ dBm. Beyond this threshold, departure from quadratic operation emerges, and the RF output voltage V_{RF} does not reflect the input voltage. It is worth noticing that at the operating point, i.e. when the transfer factor $V_B = |\partial V/\partial B|$ is at a maximum, the second harmonic signal is always at a minimum in all conditions. This is true for all frequencies, as shown in the inset of figure 7, where we

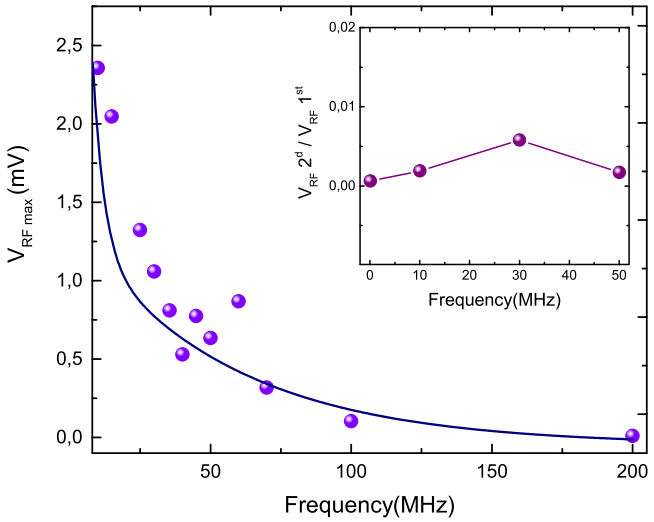

Figure 7. Maximum value of the RF signal V_{RF} (amplified) of a 1000 SQUID series SQIF as a function of the excitation frequency f_0 ranging from 25 MHz to 200 MHz, at a constant input power $P_{RF} = -55$ dBm. Temperature (67.5 K) and bias current (65 μA) are optimal. Inset: ratio of the second harmonic signal V_{RF} 2nd over the first harmonic one V_{RF} 1st $= V_{RF\max}$ as a function of the excitation frequency f_0, recorded in the same conditions than for the main panel.

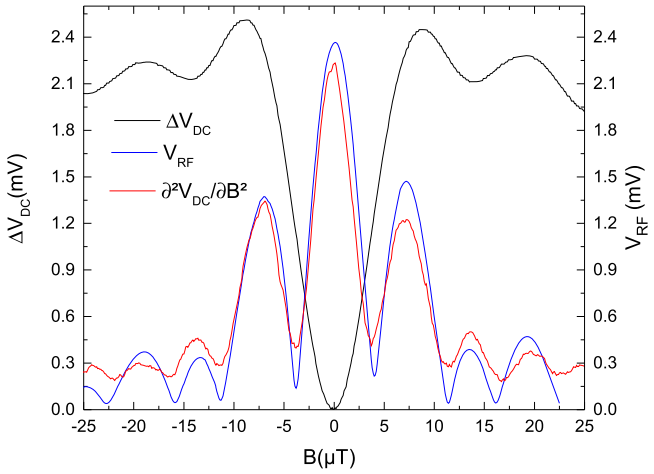

Figure 8. Simultaneous measurement of the DC ΔV_{DC} (black curve) and RF V_{RF} (blue curve) signals of a 1000 SQUID series SQIF as a function of the magnetic field B. The input RF frequency is $f_0 = 30.02$ MHz and the RF power is $P_{RF} = -30$ dBm. V_{RF} is amplified. Temperature (67.5 K) and bias current (65 μA) correspond to optimal conditions. RF is detected at $2 \times f_0 = 60.04$ MHz. The red line shows the second derivative $\partial^2 \Delta V_{DC}/\partial B^2$, which matches the RF response at $2 \times f_0$ as expected.

plotted the ratio between the second harmonic signal over the first harmonic one in optimum conditions as a function of f_0, which remains small (in the 10^{-3} range) and almost constant.

We studied in more detail the development of the non-linearity. Figure 9(a) shows $V_{RF\text{out}}$ as a function of the applied DC magnetic field B at a temperature $T = 67.2$ K and bias current $I = 70$ μA, for an AC frequency $f_0 = 101$ kHz and power P_{RF} ranging from -60 to -10 dBm. At low power, typically for $P_{RF} \leqslant -35$ dBm, a linear regime is observed: the pattern of the curve is kept constant as P_{RF} is increased, and its amplitude grows with the RF power. This can be seen by following the maximum of the curve $V_{RF\max}$ for instance. Beyond -35 dBm the curve departs from the original pattern, $V_{RF\max}$ starts saturating and then decreases as P_{RF} is increased and eventually, all structures disappear when reaching -10 dBm: this is the non-linear regime. The two regimes are observed in the second harmonic signal as well. In figure 9(b), the RF signal is plotted versus B for an excitation signal at $f_0 = 101$ kHz detected at $2 \times f_0 = 202$ kHz at different RF powers P_{RF}. The linear regime is seen below -35 dBm. The transition from a linear to non-linear regime is observed for all the frequencies studied here, and the threshold is found to be around $P_{RF} = -30$ to -35 dBm.

3. Modelling

We performed numerical simulations in order to describe in more detail the behaviour of the SQIF, in particular the transition from a linear to non-linear regime. As an example, we show here the calculations made in the case of an RF signal at frequency $f_0 = 101$ kHz (as in the data shown above), but they can be extended to all frequencies that we used. The idea is simply to add the RF and DC magnetic fields seen by the SQIF. As stated above the total field will be $B_{tot} = B + b_{RF} \sin(2\pi f_0 t)$, where B is the DC magnetic field and b_{RF} the amplitude of the RF field. We can estimate it by calculating the magnetic field produced by the RF line on the closest SQUIDs of the array:

$$b_{RF} = \left(\frac{\mu_0}{2\pi r}\right) \cdot I_{RF}$$

where r is roughly 20 μm (see figure 1) and I_{RF} is the RF current. For a circuit with an impedance matched to $Z = 50\,\Omega$, the RF power is $P_{RF} = ZI_{RF}^2$. Therefore, b_{RF} relates to P_{RF} via $b_{RF} \sim 1.5 \times 10^{-3}\sqrt{P_{RF}}$ in SI units.

We now calculate the RF signal V_{RF} measured across the SQIF. We start with the DC curve ΔV_{DC} versus B recorded simultaneously with the AC signal and presented in the inset of figure 11(b) for positive magnetic field only. A function $G(B)$ is chosen to fit it accurately (see red solid line in figure 11(b)):

$$\Delta V_{DC} = G(B) = w_0\left(1 - \frac{\sin(w_1 B)}{w_1 B}\right) - (w_2 B^2 + w_3 B + w_4)\exp(-w_5 B^2)$$

where w_i are fitting coefficients.[5]

Upon RF irradiation, we expect the total voltage across the SQIF to be $V_{tot} = G(B_{tot})$. The amplitude of the Fourier components of V_{tot} at f_0 and $2 \times f_0$ give the RF output amplitude V_{RF} and the second harmonic.

The result of the calculation is shown in figure 10, and compared to the measurements (figure 9). The main features are reproduced, such as the linear behaviour at low power and the non-monotonic behaviour of $V_{RF\max}$. To make a quantitative comparison, we introduced a single gain parameter as followed: for the lowest RF power, namely -60 dBm, we

[5] $w_0 = 1.68 \times 10^{-3}$; $w_1 = 317.2$; $w_2 = -8.545$; $w_3 = -6.11 \times 10^{-3}$; $w_4 = -1.20 \times 10^{-5}$; $w_5 = 3102$.

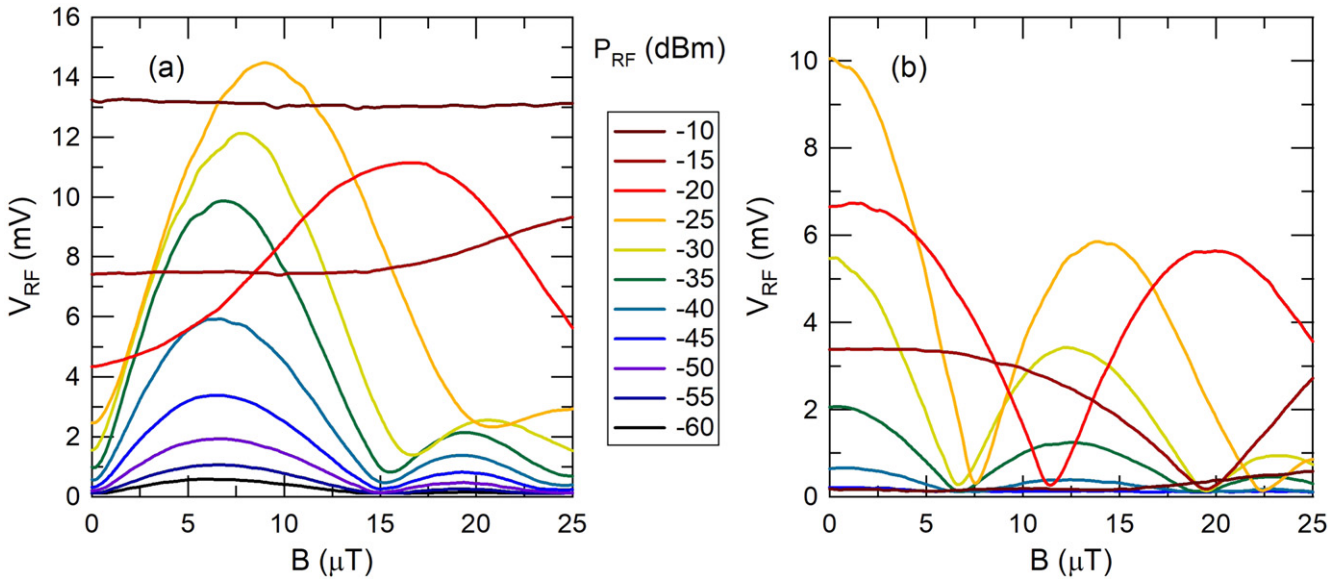

Figure 9. (a) RF signal V_{RF} (amplified) of a 1000 SQUID series SQIF as a function of the magnetic field $B \geqslant 0$ for increasing RF power P_{RF}, at temperature $T = 67.2$ K and bias current 70 μA. The frequency is $f_0 = 101$ kHz. A linear regime is observed for P_{RF} ranging from -60 to -35 dBm, while a non-linear regime is evidenced beyond—35 dBm. (b) The same behaviour is observed for the second harmonic signal.

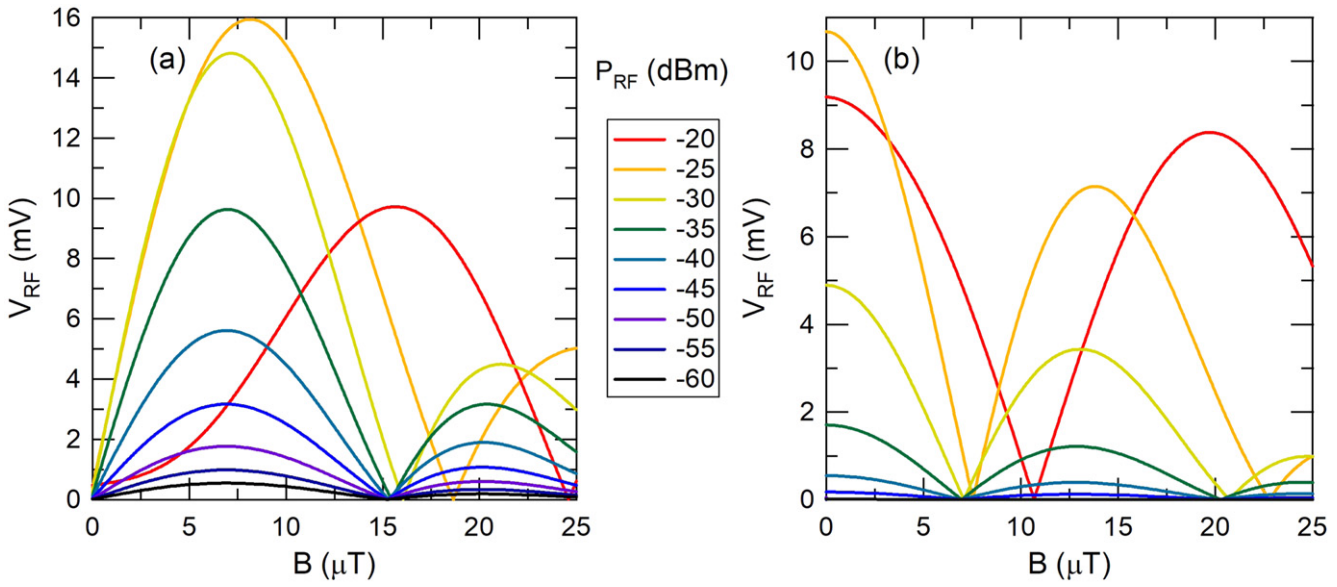

Figure 10. Simulation of the RF signal V_{RF} as a function of the magnetic field B, for different RF power P_{RF} ranging from -60 to -20 dBm (see text for details). (a) Main component. (b) Second harmonic.

made the maxima $V_{RF\max}$ coincide numerically. We then calculated the whole set of curves presented in figure 10(a). The agreement with the measured data for different RF powers is very good. This simple model shows that the non-linearity originates in the amplitude of the magnetic RF field becoming comparable to the DC one for $P_{RF} \sim -35$ dBm. Under the same assumptions, we computed the second harmonic signal, and plotted it in figure 10(b). The agreement with the data of figure 9 is also striking.

In figure 11, we plotted $V_{RF\max}$ (solid squares) and the amplitude at null DC magnetic field $V_{RF\min}$ (solid circles), as a function P_{RF} for the first (a) and the second (b) harmonic signals. The data are in blue and the computed values in red. The agreement between the calculation and the data is good for $V_{RF\max}$, but rather poor for $V_{RF\min}$: the latter increases significantly with P_{RF} in the data, while staying at almost zero in the calculation. If we focus on the second harmonic signal depicted in figure 11(b), we observe that the agreement is good both for the maximum and the minimum of the signal. Put together, this means that a significant direct inductive coupling occurs between the input RF line and the detection line, by-passing the SQIF itself. It is linear, and therefore not seen in the second harmonic signal.

We tested this hypothesis and introduced a direct coupling. The total RF voltage is now therefore: $V_{tot} = G(B_{tot}) + C \cdot b_{RF} \sin(2\pi f_0 t)$, where C is the coupling

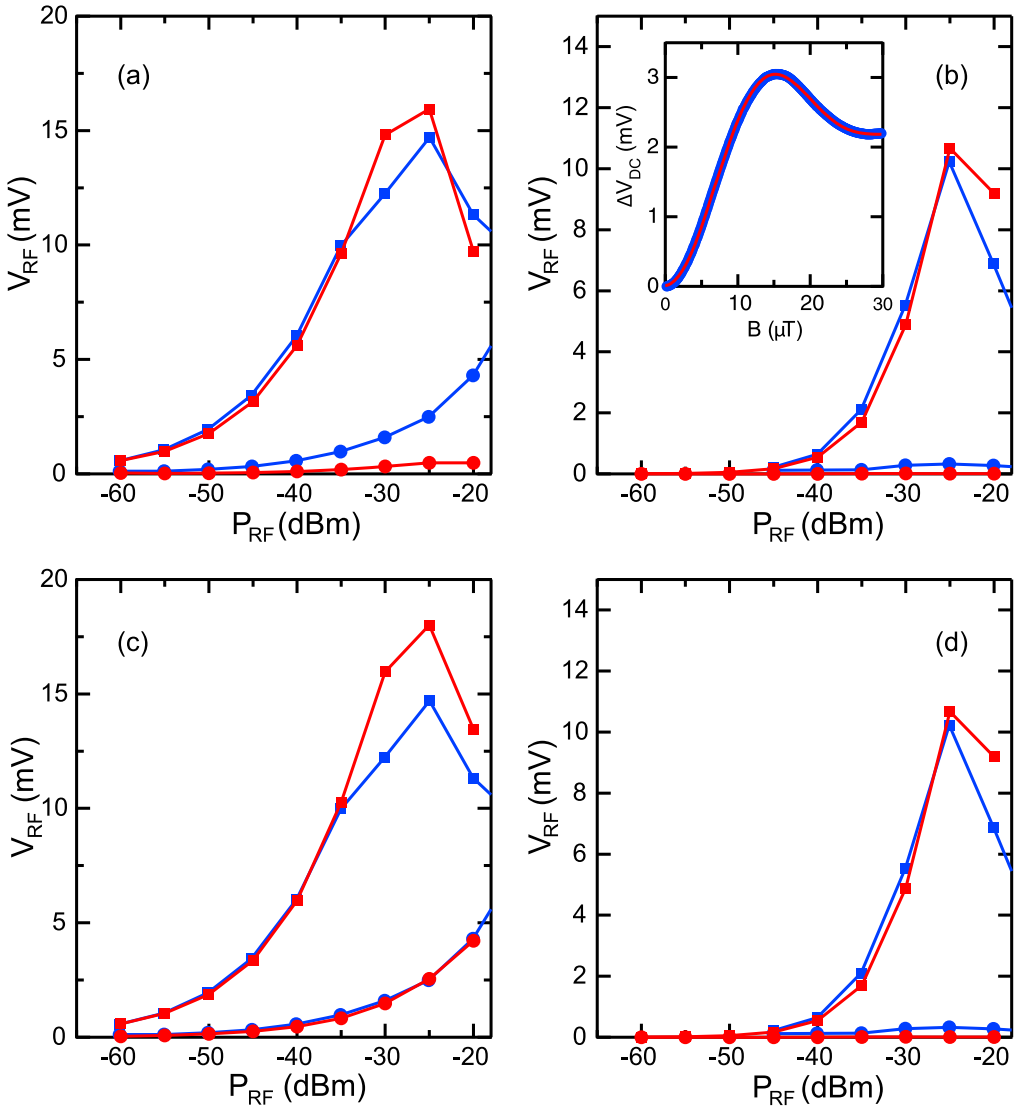

Figure 11. (a) Maximum $V_{RF\max}$ (solid squares) and minimum $V_{RF\min}$ (solid circles) of the RF voltage (amplified) as a function of the RF power P_{RF}. Data measured at $f_0 = 101$ kHz are shown in blue, and simulations in red. (b) Maximum (solid square) and minimum (solid circle) of the second harmonic RF voltage as a function of the power P_{RF}. Data are shown in blue, and simulations in red. Inset: DC response of the SQIF (ΔV_{DC} versus magnetic field B) measured while recording the AC curve with $f_0 = 101$ kHz at temperature $T = 67.2$ K and bias current $I = 70$ μA: the data are in blue and the fit function $G(B)$ used for the simulation in red. (c) Same data as in (a). The simulation now includes the direct coupling (see text). (d) Same data as in (b). The simulation now includes the direct coupling (see text).

constant that we set by matching the experimental and calculated $V_{\min}$ values at $P_{RF} = -20$ dBm ($C = 2 \times 10^{-2}$). The result is shown in figures 11(c) and (d), for the first and second harmonic signals, respectively. The agreement between the data and the computation is much better, confirming our hypothesis.

4. Conclusion

We measured the static and RF magnetic response of a HTS SQIF with 1000 SQUIDs in series, fabricated by the ion irradiation technique. A transfer factor of $\partial \Delta V_{DC}/\partial B \sim 450\,\mathrm{V\,T^{-1}}$ was achieved in DC, with a maximum swing voltage of ~2.5 mV. Coupled to a RF loop, the device presents an AC response up to 150 MHz in the experimental set-up that we used. Second harmonic generation has been shown to be at a minimum at the functioning point in the whole range of frequencies. At low RF power, over five decades below ~−35 dBm, the device operates in a linear regime, and the output signal is proportional to the input one. Beyond this value, a non-linear regime is observed, where the modulation of the AC voltage with the applied magnetic field departs from the original one. A model has been developed which is in quantitative agreement with most of the data. By analysing the differences, we showed that direct coupling to the output RF line in our set-up measurement limits the performance of the SQIF device. These results compare favourably with the ones presented in the literature for HTS SQIFs made by other methods. This shows that the ion irradiation technique provides an interesting route to make competitive HTS RF devices on a large scale.

Acknowledgments

The authors thank Yann Legall (ICUBE laboratory, Strasbourg) for ion irradiation. His work has been supported by ANRT and Thales through a CIFRE PhD fellowship No. 2015/1076, the T-SUN ANR ASTRID programme (ANR-13-ASTR-0025-01), the Emergence Programme from Ville de Paris and by the Région Ile-de-France in the framework of the DIM Nano-K and Sesame programmes.

ORCID iDs

Cheryl Feuillet-Palma https://orcid.org/0000-0002-8389-5756
Jérome Lesueur https://orcid.org/0000-0002-5843-187X

References

[1] Clarke J and Braginski A I 2005 *The SQUID Handbook: Fundamentals and Technology of SQUIDS and SQUID Systems* (Weinheim: Wiley-VCH)
[2] Welty R P and Martinis J M 1991 A series array of DC SQUIDs *IEEE Trans. Magn.* **27** 2924
[3] Drung D, Aszligmann C, Beyer J, Peters M, Ruede F and Schurig T 2005 DC SQUID readout electronics with up to 100 MHz closed-loop bandwidth *IEEE Trans. Appl. Supercond.* **15** 777–80
[4] Cybart S A, Wong T J, Cho E Y, Beeman J W, Yung C S, Moeckly B H and Dynes R C 2014 Large scale two-dimensional arrays of magnesium diboride superconducting quantum interference devices *Appl. Phys. Lett.* **104** 182604
[5] Kornev V K, Kolotinskiy N V, Sharafiev A V, Soloviev I I and Mukhanov O A 2017 From single SQUID to superconducting quantum arrays *Low Temp. Phys.* **43** 829–36
[6] Chesca B, John D and Mellor C J 2015 Flux-coherent series SQUID array magnetometers operating above 77 K with superior white flux noise than single-SQUIDs at 4.2 K *Appl. Phys. Lett.* **107** 162602
[7] Carelli P, Castellano M G, Flacco K, Leoni R and Torrioli G 1997 An absolute magnetometer based on dc superconducting quantum interference devices *Europhys. Lett.* **39** 569–74
[8] Oppenlander J, Haussler C and Schopohl N 2000 Non Φ_0 periodic macroscopic quantum interference in one-dimensional parallel Josephson junction arrays with unconventional grating structure *Phys. Rev.* B **63** 024511
[9] Oppenländer J 2003 Superconducting quantum interference filters *Adv. Solid State Phys.* **43** 731–46
[10] Cybart S A, Herr A, Kornev V and Foley C P 2017 Do multiple Josephson junctions make better devices? *Supercond. Sci. Technol.* **30** 090201
[11] Caputo P, Tomes J, Oppenlander J, Haussler C, Friesch A, Trauble T and Schopohl N 2005 Superconducting quantum interference filters as absolute magnetic field sensors *IEEE Trans. Appl. Supercond.* **15** 1044–7
[12] Schultze V, IJsselsteijn R, Meyer H-G, Oppenlander J, Haussler C and Schopohl N 2003 High-T_c superconducting quantum interference filters for sensitive magnetometers *IEEE Trans. Appl. Supercond.* **13** 775–8
[13] Oppenlander J, Caputo P, Haussler C, Trauble T, Tomes J, Friesch A and Schopohl N 2003 Effects of magnetic field on two-dimensional superconducting quantum interference filters *Appl. Phys. Lett.* **83** 969–71
[14] Schultze V, IJsselsteijn R, Boucher R, Meyer H-G, Oppenlander J, Haussler C and Schopohl N 2003 Improved high-Tc superconducting quantum interference filters for sensitive magnetometry *Supercond. Sci. Technol.* **16** 1356–60
[15] Kornev V K, Soloviev I I, Klenov N V and Mukhanov O A 2007 Development of SQIF-based output broad band amplifier *IEEE Trans. Appl. Supercond.* **17** 569–72
[16] Kornev V K, Soloviev I I, Klenov N V, Filippov T V, Engseth H and Mukhanov O A 2009 Performance advantages and design issues of SQIFs for microwave applications *IEEE Trans. Appl. Supercond.* **19** 916–9
[17] Prokopenko G V and Mukhanov O A 2013 Wideband microwave low noise amplifiers based on biSQUID SQIFs *Superconductive Electronics Conf. ISEC, IEEE* p PE7
[18] Prokopenko G V, Mukhanov O A and Romanofsky R R 2015 SQIF antenna measurement in near field *Superconductive Electronics Conf. ISEC, IEEE* SQ-P24
[19] Kornev V K, Kolotinskiy N V, Sharafiev A V, Soloviev I I and Mukhanov O A 2017 Broadband active electrically small superconductor antennas *Supercond. Sci. Technol.* **30** 103001
[20] Oppenlander J, Haeussler C, Friesch A, Tomes J, Caputo P, Traeuble T and Schopohl N 2005 Superconducting quantum interference filters operated in commercial miniature cryocoolers *IEEE Trans. Appl. Supercond.* **15** 936–9
[21] Kalabukhov A K, Chukharkin M L, Deleniv A A, Winkler D, Volkov I A and Snigirev O V 2008 Analysis of the possibility to amplify an RF signal with a superconducting quantum interference filter *J. Commun. Technol. Electron.* **53** 934–40
[22] Shadrin A V, Constantinian K Y, Ovsyannikov G A, Shitov S V, Soloviev I I, Kornev V K and Mygind J 2008 Fraunhofer regime of operation for superconducting quantum interference filters *Appl. Phys. Lett.* **93** 262503
[23] Caputo P, Tomes J, Oppenlander J, Haussler C, Trauble T and Schopohl N 2007 Two-tone response in superconducting quantum interference filters *IEEE Trans. Appl. Supercond.* **17** 722–5
[24] Caputo P, Tomes J, Oppenlander J, Haussler C, Friesch A, Trauble T and Schopohl N 2006 Quadratic mixing of radio frequency signals using superconducting quantum interference filters *Appl. Phys. Lett.* **89** 062507
[25] Mitchell E E and Foley C P 2010 YBCO step-edge junctions with high IcRn *Supercond. Sci. Technol.* **23** 065007
[26] Mitchell E E, Hannam K E, Lazar J, Leslie K E, Lewis C J, Grancea A, Keenan S T, Lam S K H and Foley C P 2016 2D SQIF arrays using 20 000 YBCO high Rn Josephson junctions *Supercond. Sci. Technol.* **29** 06LT01
[27] Katz A S, Sun A G, Woods S I and Dynes R C 1998 Planar thin film YBCO Josephson junctions via nano-lithography and ion damage *Appl. Phys. Lett.* **72** 2032–4
[28] Bergeal N, Grison X, Lesueur J, Faini G, Aprili M and Contour J P 2005 High-quality planar High T_c Josephson junctions *Appl. Phys. Lett.* **87** 102502
[29] Malnou M *et al* 2012 Toward terahertz heterodyne detection with superconducting Josephson junctions *Appl. Phys. Lett.* **101** 233505
[30] Malnou M, Feuillet-Palma C, Ulysse C, Faini G, Febvre P, Sirena M, Olanier L, Lesueur J and Bergeal N 2014 High-Tc superconducting Josephson mixers for terahertz heterodyne detection *J. Appl. Phys.* **116** 074505
[31] Sharafiev A, Malnou M, Feuillet-Palma C, Ulysse C, Wolf T, Couëdo F, Febvre P, Lesueur J and Bergeal N 2018 HTS

Josephson junctions arrays for high-frequency mixing *Supercond. Sci. Technol.* **31** 035003
[32] Cybart S A, Wu S M, Anton S M, Siddiqi I, Clarke J and Dynes R C 2008 Series array of incommensurate superconducting quantum interference devices from YBCO ion damage Josephson junctions *Appl. Phys. Lett.* **93** 182502
[33] Cybart S A, Anton S M, Wu S M, Clarke J and Dynes R C 2009 Very large scale integration of nano-patterned YBCO Josephson junctions in a two-dimensional array *Nano Lett.* **9** 3581–5
[34] Cybart S A, Dalichaouch T N, Wu S M, Anton S M, Drisko J A, Parker J M, Harteneck B D and Dynes R C 2012 Comparison of measurements and simulations of series-parallel incommensurate area superconducting quantum interference device arrays fabricated from $YBa_2Cu_3O_{7-\delta}$ ion damage Josephson junctions *J. Appl. Phys.* **112** 063911
[35] Ouanani S *et al* 2014 HTS ion damage Josephson junction technology for SQUID arrays *J. Phys.: Conf. Ser.* **507** 042008
[36] Ouanani S, Kermorvant J, Ulysse C, Malnou M, Lemaître Y, Marcilhac B, Feuillet-Palma C, Bergeal N, Crété D and Lesueur J 2016 High-Tc superconducting quantum interference filters (SQIFs) made by ion irradiation *Supercond. Sci. Technol.* **29** 094002
[37] Bergeal N, Lesueur J, Faini G, Aprili M and Contour J P 2006 High T_c superconducting quantum interference devices made by ion irradiation *Appl. Phys. Lett.* **89** 112515
[38] Bergeal N, Lesueur J, Sirena M, Faini G, Aprili M, Contour J P and Leridon B 2007 Using ion irradiation to make High T_c Josephson junctions *J. Appl. Phys.* **102** 083903
[39] Katz A S, Woods S I and Dynes R C 2000 Transport properties of high-Tc planar Josephson junctions fabricated by nano-lithography and ion implantation *J. Appl. Phys.* **87** 2978
[40] Ouanani S 2015 Etude de réseaux de jonctions Josephson à haute température critique *PhD Thesis* Université Paris-Sud
[41] Wu S, Cybart S, Anton S M and Dynes R C 2013 Simulation of series arrays of superconducting quantum interference devices *IEEE Trans. Appl. Supercond.* **23** 1600104